The Astrophysical Journal, 689: L69–L72, 2008 December 10


# CRISP SPECTROPOLARIMETRIC IMAGING OF PENUMBRAL FINE STRUCTURE

G. B. Scharmer,[1] G. Narayan,[1,2] T. Hillberg,[1,2] J. de la Cruz Rodriguez,[1,2] M. G. Löfdahl,[1] D. Kiselman,[1] P. Sütterlin,[1] M. van Noort,[1] and A. Lagg[3]

*Received 2008 June 10; accepted 2008 October 17; published 2008 November 3*

## ABSTRACT

We discuss penumbral fine structure in a small part of a pore, observed with the CRISP imaging spectropolarimeter at the Swedish 1-m Solar Telescope (SST), close to its diffraction limit of 0.16″. Milne-Eddington inversions applied to these Stokes data reveal large variations of field strength and inclination angle over dark-cored penumbral intrusions and a dark-cored light bridge. The mid-outer part of this penumbra structure shows ∼0.3″ wide spines, separated by ∼1.6″ (1200 km) and associated with 30° inclination variations. Between these spines, there are no small-scale magnetic structures that easily can be identified with individual flux tubes. A structure with nearly 10° more vertical and *weaker* magnetic field is seen midway between two spines. This structure is cospatial with the brightest penumbral filament, possibly indicating the location of a convective upflow from below.

*Subject headings:* magnetic fields — sunspots

## 1. INTRODUCTION

The discovery of dark cores in sunspot penumbral filaments (Scharmer et al. 2002) suggests that the basic elements of penumbral fine structures are observable. The nature of individual dark cores was investigated with high-resolution multiline spectra, but without polarization information, by Bellot Rubio et al. (2005). They concluded that the cores are associated with weaker magnetic field strength, by 100–300 G. Langhans et al. (2007) measured the azimuthal variation of circular polarization signal in the 6302 Å Fe I line of regular spots at different heliocentric distances. They found that dark cores are associated with a *strongly* reduced field strength and a magnetic field that is more horizontal than for their lateral brightenings by about 10°–15°. Analysis of spectropolarimetric data from the Japanese satellite *Hinode* also shows lower field strength in the dark cores, but only by 100–150 G, and small inclination changes of about 4° (Bellot Rubio et al. 2007).

We describe the first spectropolarimetric observations with CRISP, an imaging spectropolarimeter built for the Swedish 1-m Solar Telescope (SST). The large, unobscured aperture of the SST corresponds to a diffraction-limited resolution that is twice as high as that of *Hinode*. We present CRISP observations of penumbral fine structure made at a spatial resolution close to the SST diffraction limit of 0.16″. Using Milne-Eddington (ME) inversions applied to these data, we discuss spatial variations of the magnetic field and line-of-sight (LOS) velocities for penumbral structure seen over parts of a large pore.

## 2. OBSERVATIONAL DATA AND PROCESSING

CRISP is a spectropolarimeter, based on a dual Fabry-Pérot interferometer (FPI) system similar to that described by Scharmer (2006). The spectral resolution is modest (about 60 mÅ at 6302 Å), to limit the number of wavelengths needed without aliasing and to allow a large field of view (FOV) at high image quality. The present image scale is 0.071″ pixel$^{-1}$. Further information about CRISP will be given in a future publication.

For polarimetric analysis, a polarizing beam splitter close to the final focal plane is used with two 1k × 1k pixel$^2$ synchronized CCDs and nematic liquid crystals (LCs). For image restoration, a third CCD simultaneously records a wide-band image through the prefilter of the FPI system.

The data discussed in this Letter were recorded on 2008 April 22 at approximately 11:58 UT. The target was two large pores of opposite polarities (AR 10992), located at approximately N18 E4, corresponding to a heliocentric distance of approximately 19° ($\mu = 0.94$). We discuss data from a small part of one of these pores, indicated by the larger of the two boxes shown in Figure 1.

The images recorded correspond to complete Stokes measurements at 11 line positions in steps of 48 mÅ, from −240 to +240 mÅ, in the Fe I line at 6302 Å. In addition, images were recorded at one continuum wavelength. The frame rate was 36 Hz, with an exposure time of 16 ms and a CCD readout time of 10 ms. For each wavelength and LC state, 14 images were recorded per camera. Each sequence processed consists of about 630 images per CCD (1890 images in total) and was recorded during a total time interval of 22 s. The images, covering a FOV of 71″ × 71″, were divided into overlapping 128 × 128 pixel$^2$ subfields and all images from each subfield were processed with MOMFBD image restoration techniques (van Noort et al. 2005). To further reduce noise, two consecutive sets of images were aligned and co-added. These images were demodulated with respect to the polarimeter (pixel by pixel) and the telescope polarization model developed by Selbing (2005)—for details, see also van Noort & Rouppe van der Voort (2008). In addition, the Stokes images were corrected for remaining $I$ to $Q$, $U$, and $V$ cross talk with the aid of the Stokes images recorded in the continuum. The final Stokes images thus obtained were combined to Stokes spectra. It was verified that nearly all Stokes $V$ profiles are normal with two lobes and small asymmetries, justifying the use of ME inversion techniques with this data. Stokes $Q$, $U$, and $V$ images were further inspected for evidence of cross talk from $V$ to $Q$ or $U$ but several examples of strong $V$ features without cospatial $Q$ or $U$ features seen in the 2D maps suggest that such cross talks must be small. We finally estimated the noise level to be ap-

[1] Institute for Solar Physics, Royal Swedish Academy of Sciences, AlbaNova University Center, SE-106 91 Stockholm, Sweden.
[2] Stockholm Observatory, Stockholm University.
[3] Max Planck Institute for Solar System Research, Max-Planck-Strasse 2, DE-37191 Katlenburg-Lindau, Germany.

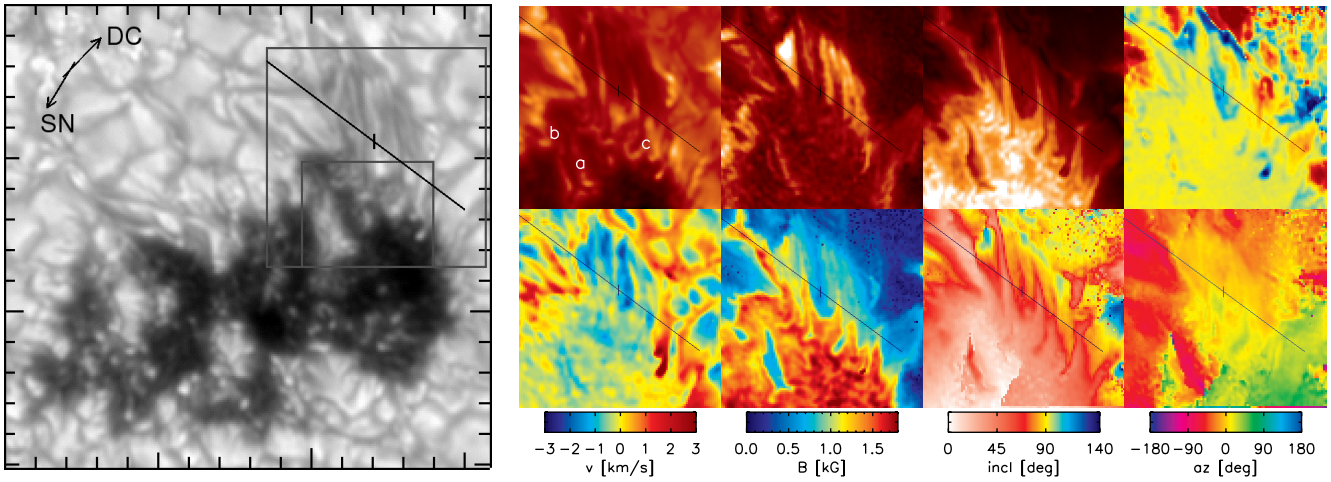


FIG. 1.—*Left*: The continuum image of one of the two pores observed with CRISP. The upper right part of this pore and the associated light-bridge structure and penumbral filaments, indicated with the large box, are discussed in this Letter. The directions of solar disk center (DC) and solar north (SN) are indicated with arrows. Tick marks are separated by 1″. *Right*: The top row shows Stokes *I* at line center, the integrated linear and circular polarization, and the Stokes *V* area asymmetry (AA). The color coding of AA is such that yellow indicates small AA, green-blue negative AA (Stokes *V* is negative in the blue wing over most of the spot), and red positive AA. The bottom row shows the LOS velocity, field strength, inclination, and azimuth angles derived from the inversions. The dark line indicates the cut along which plots are shown in Fig. 4. The size of the boxes are ~7.1″ × 7.1″.

proximately $1.0 \times 10^{-3}$ for Stokes *V* and $1.1 \times 10^{-3}$ for Stokes *Q* and *U*. For the analysis presented here, no attempt was made to compensate for the telluric blend; instead the Stokes data obtained at +240 mÅ were ignored. Also, any FOV variations of the *shape* of the FPI transmission profile from cavity errors in the two etalons were ignored and the theoretical profile based on known cavity separations and reflectivities was used. Examples of observed and the corresponding calculated Stokes profiles are shown in Figure 2.

The final Stokes images were processed with the ME inversion software HELIX, developed by Lagg et al. (2004). The following parameters were determined by the code: LOS velocity, Doppler width, the gradient of the source function and the field strength *B*, inclination and azimuth angle of the magnetic field, plus a parameter allowing adjustment of the continuum level. Macroturbulence was set to zero. The ratio of line center to continuum opacity, $\eta_0$, was set to 16, the damping parameter to 1, and the filling factor *f* to 1. Because of the assumed unit filling factor, the derived magnetic field parameters represent locally averaged values, also along the LOS. The filling factor was fixed at unity for comparison with the inversions of Bellot Rubio et al. (2007), discussed in § 3.2. Tests with free *f* showed a few localized areas with strongly reduced *f* and strongly increased *B* but the average field strength, *Bf*, was consistently close to what was obtained with $f = 1$. Allowing $\eta_0$ to vary gave large changes in the source function gradient but had small effect on the magnetic field. These tests and tests with other inversion codes convinced us that the inversion results are robust.

Finally, we used the flat-field images, recorded at steps of 24 mÅ and based on images accumulated during 40 minutes, to produce a 6302 Fe I line etalon cavity map, corresponding to the Doppler shift bias introduced by the cavity errors. This bias was subtracted from the Doppler shifts derived by the inversion software. After this correction, the average Doppler shifts of the two pores differed by about 60 m $s^{-1}$. The average of the two pore Doppler shifts were used as reference for all velocities measured. We used this calibration to calculate the average convective blueshift of the part of the surrounding quiet Sun that showed no magnetic field significantly above the noise level. The convective blueshift thus obtained was 210 m $s^{-1}$. This is close to the value obtained for this line from convection simulations at a heliocentric distance of 19°, −236 m $s^{-1}$ by J. de la Cruz Rodriguez (in preparation), but differing by 130 m $s^{-1}$ from the value obtained by Domínguez Cerdeña et al. (2006).

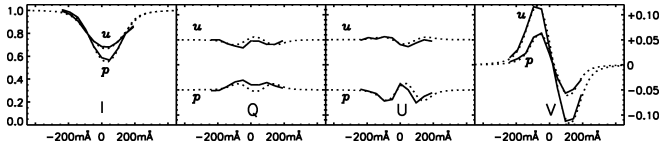


FIG. 2.—Two sets of observed (*solid line*) and fitted (*dotted line*) Stokes profiles from the umbra (u) and penumbra (p). Stokes *Q*, *U*, and *V* are normalized to the continuum intensity and plotted on the same scale, but with *Q* and *U* shifted vertically for clarity.

## 3. RESULTS

Figure 1 (*right panel*) shows input data and results of the inversions. The total linear and circular polarizations are calculated as $\int (Q^2 + U^2)^{1/2} d\lambda / I_c$ and $\int |V| d\lambda / I_c$, where $I_c$ is the continuum intensity, and the Stokes *V* area asymmetry as $\int V d\lambda / \int |V| d\lambda$.

### 3.1. *Dark-Cored Structures*

A short irregular light bridge, labeled "a," and four dark-cored intrusions are seen in the pore. The dark cores are barely visible in the continuum Stokes *I* image but clearly visible in line center Stokes *I*, the integrated circular polarization and the field strength maps. The light bridge dark core "a" and the two strongest dark-cored intrusions, labeled "b" and "c," show clear variations in the inclination and azimuth angle. The light bridge dark core "a" and one of the other dark cores split up in Y-shapes at their innermost parts, similar to what was first reported by Scharmer et al. (2002) and also seen in umbral dot simulations by Schüssler & Vögler (2006). Figure 3 shows the horizontal magnetic field component for every second pixel within the small box in Figure 1, after resolving the 180° ambiguity and transforming the magnetic field to the solar local reference frame. The light-bridge dark core "a" and the stron-

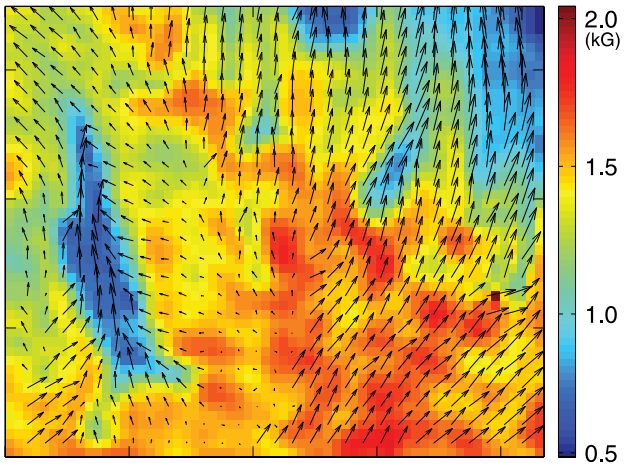


FIG. 3.—The horizontal magnetic field component within the small box shown in Fig. 1, overlaid on the field strength map. Large variations in the azimuthal angle are associated with the light bridge and the most prominent dark core associated with penumbral filaments. Tick marks are separated by 1″.

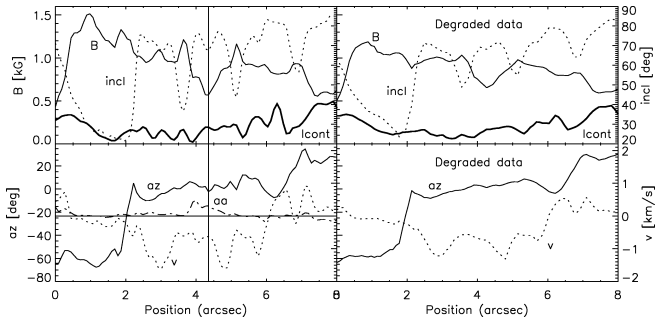


FIG. 4.—The inclination angle, azimuth angle, LOS velocity, field strength, continuum intensity, and Stokes *V* area asymmetry (AA) along the line shown in Fig. 1, with the mark midway corresponding to the vertical line shown in the present figure. AA uses the same scaling as the LOS velocity in the right-hand side of the figure. *Left*: Inversions based on SST data. *Right*: Inversions based on SST data degraded to a resolution corresponding to a 50 cm telescope with 34% linear obscuration.

gest dark-cored intrusion "c" are associated with a magnetic field that is more horizontal, weaker, and aligned with the main axis of the dark cores. The minimum field strength in these dark cores is approximately 600–800 G, as compared to the average field strength in the pore of 1600 G and a peak field strength of 2100 G. Crossing the dark core of the light bridge ("a"), the inclination angle varies by over 50° and by approximately 15° when crossing the dark core of "c." However, for neither of these dark cores is the magnetic field close to horizontal. For dark cores "a," "b," and "c," the maximum inclinations are 70°, 60°, and 55°, respectively. Figure 3 shows large variations, by nearly 90°, in the magnetic field azimuth angle across the light bridge dark core and 45° variations across the dark core of "c," The magnetic field for both these dark cores is aligned with the main axis of the cores. The Doppler map shows blueshifts of 0.6 km $s^{-1}$ in the light bridge structure, and about 0.3 km $s^{-1}$ along the core.

### 3.2. *Penumbra Spine Structures*

The penumbral filamentary structures seen farther away from the center of the pore show only a single thin dark core. Other filamentary structures are similar to those of the outer parts of mature penumbrae. Figure 4 shows plots of the inclination angle, azimuth angle, LOS velocity, field strength, continuum intensity, and Stokes *V* area asymmetry (AA, labeled "aa" in the plot) along the thin black line in Figure 1. As can be seen, AA is small except close to one of the spines. The most prominent variations are those of the inclination, varying by up to 40° over distances of only 0.25″–0.3″. In contrast, the azimuth angle varies by only ±7°. The plot and Figure 1 also show spines (dark structures in the inclination map), first identified by Lites et al. (1993), associated with small, on the order of 150 G, enhancements of the field strength in the inner and mid parts of the spines. Along the spines, the field strength and inclination variations appear as radial extensions of the stronger and more vertical field of the umbral part of the pore. The FWHM of the spines, as measured from the inclination map, is in the range 0.25″–0.35″. In the outer parts of this penumbra, the field strength of the spines is very close to that of their surroundings. This field strength variation with radial distance is qualitatively similar to that reported by Westendorp Plaza et al. (2001), derived from ASP data obtained at much lower spatial resolution. The LOS velocity shows large variations. Where the magnetic field is more horizontal, the LOS blueshift is around 1.2–1.7 km $s^{-1}$ and where it is more vertical, it is approximately 0.3–0.4 km $s^{-1}$. Figures 1 and 4 show a weak spinelike structure, indicated with a short dark vertical line in Figure 1, in the inclination map. Here the magnetic field is more vertical than in the immediate surroundings, but only by less than 10°, and the field strength reaches a local *minimum* in contrast to what is the case for the two spines surrounding this structure. This feature can be seen clearly as a "gap" in the integrated linear polarization map shown in Figure 1 and it shows up in all ME inversions made, including those with free filling factor. Thus we see spinelike structures associated with a more vertical field of two types: those that are associated with stronger field in the mid-inner penumbra and those that are associated with weaker field throughout the penumbra. Similar conclusions were first drawn by Westendorp Plaza et al. (2001, cf. their Fig. 11). However, the present data show no obvious evidence of field lines spreading in the azimuthal direction away from the spines, as found for filaments close to the symmetry axis on the limb side by Borrero et al. (2008). Along the structure with minimum field strength, the LOS blueshift is strongly reduced to only about 0.3 km $s^{-1}$. This region of minimum field strength corresponds to the brightest penumbral filament seen in the continuum image.

Another notable feature is the variation of the inclination along the edge outlining the outer penumbral boundary. Along this edge the inversions return inclinations close to 90°, with some local inclinations as large as 100°, suggesting field lines that return down into the photosphere at shallow angle with respect to the surface. Redshifts in the range 0.6–1.0 km $s^{-1}$ are seen here. Several examples of abnormal (single- or multilobed) Stokes *V* profiles are found within this region. A localized, very strong redshift, most likely to be a downflow, can be seen associated with a narrow filamentary intrusion in the lower right part of Figure 1. At the location of the peak redshift, the Stokes profiles are sufficiently shifted in wavelength that the inversions cannot be trusted. Here, Stokes *V* profiles are strongly asymmmetric or abnormal with one or three lobes. It is likely that the LOS velocity exceeds 5 km $s^{-1}$ in this region. Similar strong downflows at the edge of umbrae were recently reported by Shimizu et al. (2008).

The spatial variations in the inferred properties of the magnetic field are in qualitative agreement with findings from inversions of *Hinode* Stokes data (Bellot Rubio et al. 2007), but

at the high spatial resolution of the present data, some of these variations are found to be significantly larger. We have estimated the effect of higher spatial resolution by degrading the resolution of the present SST data to that of a 50 cm telescope with a linear central obscuration of 34%. We binned the data over $2 \times 2$ pixel$^2$ to a pixel size of $0.14''$. This process gives an impression of the improvement gained by the larger aperture of the SST over a 50 cm telescope such as *Hinode* SOT. Inversions based on this degraded data are shown in the right panel of Figure 4. This demonstrates a reduction of the inclination variations across the spines of about 50%. Small-scale variations in field strength and LOS velocity are reduced by more than 50% but large-scale variations remain intact, suggesting (as confirmed by other tests discussed above) that the inversions are robust. The minimum field strength for the light bridge is increased only marginally, but for dark cores "b" and "c," the increase is from 720 to 980 G and from 780 to 1040 G, respectively. The maximum inclination angles are decreased from 70° to 50° ("a"), from 60° to 48° ("b"), and from 55° to 50° ("c"). This strongly suggests that the inferred stronger variations in magnetic field properties across spines, a dark-cored light bridge and dark-cored filaments, compared to what is obtained from *Hinode* data (Bellot Rubio et al. 2007), are to a large extent due to the higher spatial resolution of the present data.

## 4. DISCUSSION

We have presented ME inversions based on data obtained with the CRISP imaging spectropolarimeter, used with the 1 m SST. The spatial resolution of this Stokes data represents a breakthrough in ground-based spectropolarimetry and a major improvement also as compared to recent *Hinode* data. The large variations in field strength and inclination angle inferred from the present data can to a large extent can be explained with the high spatial resolution of the SST CRISP data.

The penumbra observed is partial, covering only a small part of the pore observed. We have analyzed dark-cored filamentary structures intruding into this pore and a light-bridge-like structure, detached from the surrounding photosphere. The three dark-cored structures analyzed are associated with strongly reduced field strength (around 50% relative to their surroundings), and a significantly more horizontal magnetic field (by 15°–50°) than outside the dark cores. The variations in field strength and inclination across the dark-cored filament are consistent with analysis of earlier SST magnetogram (Stokes *V*) data (Langhans et al. 2007). Even with the high spatial resolution of that and the present SST data, the magnetic field is found to be far from horizontal above the penumbral dark cores.

The inclination map shows a pronounced "spine" structure (Lites et al. 1993) with a magnetic field that is locally more vertical by ~30° and that, except in the outer penumbra, is locally stronger by about 150 G. Within these spines, the LOS velocities are strongly reduced. The spines seen in Figure 1 are separated by about 1200 km. Such widely separated spines were evident also in earlier SST magnetogram data, discussed by Scharmer et al. (2007). We do not find any evidence for horizontal flux tubes with diameters in the range 100–250 km modeled in numerous papers (e.g., Borrero et al. 2007; Tritschler et al. 2007; Ruiz Cobo & Bellot Rubio 2008), in the outer penumbra. Midway between two of the spines, a faint spinelike structure is seen in the inclination map. The locally weaker and more *vertical* magnetic field of this structure is in contradiction with an interpretation in terms of a horizontal flux tube. The region with weaker field strength coincides with the brightest penumbral filament seen in the continuum. A possible interpretation is that the faint spinelike structure is related to a weak convective upflow, making the magnetic field overlying that upflow locally more vertical. This interpretation must be regarded as speculative in view of the small LOS velocities measured. Future CRISP observations of larger sunspots are likely to clarify this and also to provide more critical constraints on models.

The Swedish 1-m Solar Telescope is operated on the island of La Palma by the Institute for Solar Physics of the Royal Swedish Academy of Sciences in the Spanish Observatorio del Roque de los Muchachos of the Instituto de Astrofísica de Canarias. CRISP was funded by the Marianne and Marcus Wallenberg Foundation. JdlCR was supported by a Marie Curie Early Stage Research Training Fellowship of the European Community's Sixth Framework Programme under contract number MEST-CT-2005-020395: The USO-SP International Graduate School for Solar Physics.

*Facilities*: SST(CRISP)

## REFERENCES

Bellot Rubio, L. R., Langhans, K., & Schlichenmaier, R. 2005, A&A, 443, L7
Bellot Rubio, L. R., et al. 2007, ApJ, 668, L91
Borrero, J. M., Bellot Rubio, L. R., Müller, D. A. N. 2007, ApJ, 666, L133
Borrero, J. M., Lites, B. W., & Solanki, S. K. 2008, A&A, 481, L13
Domínguez Cerdeña, I., Almeida, J. S., & Kneer, F. 2006, ApJ, 646, 1421
Lagg, A., Woch, J., Krupp, N., & Solanki, S. K. 2004, A&A, 414, 1109
Langhans, K., Scharmer, G. B., Kiselman, D., Löfdahl, M. G. 2007, A&A, 464, 763
Lites, B. W., Elmore, D. F., Seagraves, P., & Skumanich, A. P. 1993, ApJ, 418, 928
Ruiz Cobo, B., & Bellot Rubio, L. R. 2008, A&A, 488, 749
Scharmer, G. B. 2006, A&A, 447, 1111
Scharmer, G. B., Gudiksen, B. V., Kiselman, D., Löfdahl, M. G., & Rouppe van der Voort, L. H. M. 2002, Nature, 420, 151
Scharmer, G. B., Langhans, K., Kiselman, D., & Löfdahl, M. G. 2007, in ASP Conf. Ser. 369, New Solar Physics with *Solar-B* Mission, ed. K. Shibata et al. (San Francisco: ASP), 71
Schüssler, M., & Vögler, A. 2006, ApJ, 641, L73
Selbing, J. 2005, M.S. thesis, Stockholm Univ.
Shimizu, T., et al. 2008, ApJ, 680, 1467
Tritschler, A., Müller, D. A. N., Schlichenmaier, R., & Hagenaar, H. J. 2007, ApJ, 671, L85
van Noort, M. J., & Rouppe van der Voort, L. H. M. 2008, A&A, 489, 429
van Noort, M. J., Rouppe van der Voort, L. H. M., & Löfdahl, M. G. 2005, Sol. Phys., 228, 191
Westendorp Plaza, C., del Toro Iniesta, J. C., Ruiz Cobo, B., Pillet, V. M., Lites, B. W., & Skumanich, A. 2001, ApJ, 547, 1130